Title

Ab initio
computation for solid-state
31
P NMR of inorganic phosphates: revisiting X-ray structures

Journal

Physical Chemistry Chemical Physics, 21(19)

ISSN

1463-9076 1463-9084

Authors

Pilar, Kartik
Deng, Zeyu
Preefer, Molleigh B
et al.

Publication Date

2019

DOI

10.1039/C9CP01420A

Peer reviewed

Journal Name

ARTICLE TYPE

Cite this: DOI: 00.0000/xxxxxxxxxx

Ab initio computation for solid-state ^{31}P NMR of inorganic phosphates: Revisiting X-ray structures†

Kartik Pilar,[a] Zeyu Deng,[b] Molleigh B. Preefer,[a,c] Joya A. Cooley,[a] Raphaële Clément,[a,d] Ram Seshadri,[a,c,d] and Anthony K. Cheetham[a,e*]

Received Date
Accepted Date

DOI: 00.0000/xxxxxxxxxx

The complete ^{31}P NMR chemical shift tensors for 22 inorganic phosphates obtained from *ab initio* computation are found to correspond closely to experimentally obtained parameters. Further improvement was found when structures determined by diffraction were geometry optimized. Besides aiding in spectral assignment, the cases where correspondence are significantly improved upon geometry optimization point to the crystal structure requiring correction.

1 Introduction

Magnetic resonance spectroscopy is widely employed for probing the structure of materials. The strong dependence of the NMR chemical shift on the surrounding chemical environment provides a sensitive probe to local structure around atoms. However, a certain degree of difficulty arises in the interpretation of solid-state NMR spectra when there is more than one crystallographic site for the element of interest and those sites have the same multiplicity. In such cases the assignment of peaks to particular sites can be challenging.

Several methods have been used for determining solid-state NMR peak assignments. Before the advent of high performance computing, Smith *et al.* reported a linear correlation between easily calculated oxygen bond-strength sums and ^{29}Si isotropic chemical shifts in silicates.[2] This method was later extended by Cheetham *et al.* to the ^{31}P chemical shifts of 22 different inorganic phosphates: a recreation of the correlation they found is presented in Figure 1(a).[1]

With growing access to high performance computing, more precise computational methods have become common for the assignment of solid-state NMR shifts. For example, correlation between chemical shifts and the computed Bader charges on atoms are sometimes found to be useful.[3,4] In the context of this work, we have used standard computational routines[5] to compute Bader charges on ^{31}P atoms, and found that almost no correlation [data presented in Figure 1(b)] is observed for the ^{31}P chemical shifts on the set of phosphates investigated by Cheetham *et al.*[1]

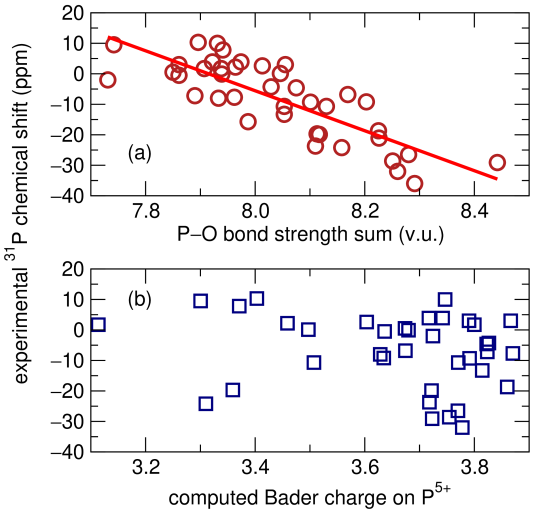

Fig. 1 (a) Oxygen bond strength sums plotted against experimental isotropic ^{31}P solid-state NMR chemical shifts recreated using data originally reported by Cheetham *et al.*[1] $R^2 = 0.666$. (b) No relationship was found between chemical shift and Bader charge on the same set of phosphates.

Cluster models employing gauge-including atomic orbitals have been used to predict chemical shifts.[6,7] However, this type of cluster approximation can lead to issues in relation to cluster termination,[8] as the cutoff at which interatomic interactions on the probed nucleus can be considered negligible is non-trivial.

In 2001, Mauri and Pickard developed the gauge-including projector augmented wave (GIPAW) formalism using periodic bound-

[a]*Materials Research Laboratory, University of California Santa Barbara, California 93106 United States.*
[b]*Department of Materials Science and Metallurgy, University of Cambridge 27 Charles Babbage Rd, CB3 0FS Cambridge, UK*
[c]*Department of Chemistry and Biochemistry, University of California Santa Barbara, California 93106 United States.*
[d]*Materials Department, University of California Santa Barbara, California 93106 United States*
[e]*Department of Materials Science and Engineering, National University of Singapore Singapore 117575, Singapore*
* E-mail: akc30@cam.ac.uk
† Electronic Supplementary Information (ESI) available. See DOI: 00.0000/00000000.

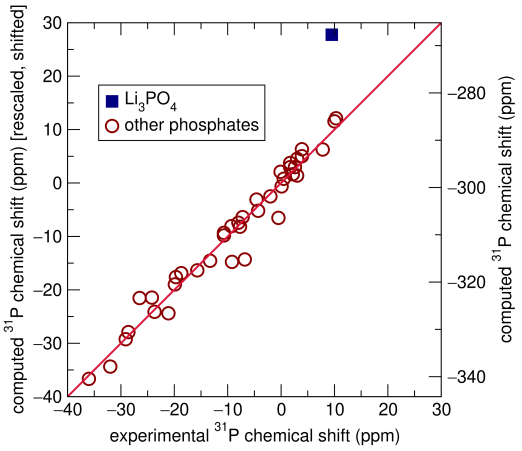

Fig. 2 GIPAW-calculated isotropic chemical shifts using reported structures from ICSD compared to experimentally reported values. $R^2 = 0.928$, or $R^2 = 0.963$ if Li_3PO_4 is disregarded. Raw calculated data are displayed on the right vertical axis, while the left vertical axis is rescaled by a factor of 0.886 and shifted 265.08 ppm to correspond to experimental results.

ary conditions, thereby averting the issue of cluster termination.[9,10] Their method included a linear transformation using projectors to reconstruct the all-electron density at the atomic core from the prescribed pseudopotential. The response of the electron density to an imposed magnetic field can be subsequently calculated. The core contribution to this magnetic shielding is independent from the surrounding chemical environment,[11] so the core shielding contribution need only be calculated a single time, thereby saving significant computational resources over the all-electron approach.[12] The GIPAW approach was first used for NMR spectral assignments by Profeta and coworkers in silicates[13] and has since been applied to a wide range of organic and inorganic compounds, including sodium perovskites,[14] organic solids,[15,16] aluminum oxides,[17] and phosphates.[18–26]

2 Computational methods

The present work utilizes the GIPAW methodology as a more precise method of computing ^{31}P NMR chemical shift assignments for the set of inorganic phosphates previously reported by Cheetham *et al.*,[1] with the aim of more precisely predicting NMR chemical shifts for the 22 phosphate phases, only two of which have been previously studied in this manner.[20] All experimental data presented here has been taken from this previous work by Cheetham and coworkers.

Three separate sets of calculations were completed using the GIPAW formalism to compute chemical shift tensors. The Vienna Ab initio Simulation Package (VASP) software was used to perform all calculations.[27,28] The PBEsol generalized gradient approximation (GGA) functional was used to model electron correlation effects[29] although calculations using the PBE functional (data presented in the supplementary information†) yield similar results. Previous GIPAW studies of NMR parameters have almost exclusively made use of the PBE functional; however, here we demonstrate minor improvement while using PBEsol. Dispersion forces were not taken into account. Automatically generated γ-centered k-point grids of varying sizes were used to sample the Brillouin zone based upon unit cell dimensions.† The first set of GIPAW computations was carried out on structures obtained directly from the Inorganic Crystal Structure Database (ICSD),[30–51] using a plane-wave basis set cut-off energy of 800 eV. A second and third set of chemical shift calculations were also completed on DFT geometry optimized structures: one set in which atomic positions were allowed to relax but lattice parameters were kept rigid at the X-ray determined values and the other on structures which were fully relaxed. The plane-wave basis set cut-off energy was set to 500 eV for relaxations, although 800 eV was still used for subsequent chemical shift computations. DFT relaxations minimize structural energy and can lead to more precise atomic positions than can be obtained from X-ray diffraction, especially when referencing older crystallographic reports or when light elements are present in the compound,[52] which is the case for most of the compounds being investigated in this work.

3 Results and Discussion

Chemical shift tensors are second rank 3×3 matrices, which can be diagonalized and described in Herzfeld-Berger notation by three parameters: isotropic chemical shift, δ_{iso}, span, Ω, and skew, κ, defined as:

$$\delta_{iso} = \frac{\delta_{11} + \delta_{22} + \delta_{33}}{3} \quad (1)$$

$$\Omega = \delta_{11} - \delta_{33} \quad (2)$$

$$\kappa = \frac{3(\delta_{22} - \delta_{iso})}{\Omega} \quad (3)$$

where δ_{xx} are the components of the diagonalized chemical shift tensor. The most common method of NMR spectral assignment is via the analysis of the isotropic chemical shift. It is observed that for all structures investigated here, the computed isotropic chemical shifts were highly correlated with experimentally determined values. The R^2 value between computed and experimental isotropic chemical shifts was found to be 0.928 for computations carried out on structures taken directly from the database, as shown in Figure 2. Li_3PO_4 is a clear outlier in this data set, with a computed shift of 27.8 ppm, referenced, and an experimental isotropic shift of 9.5 ppm. Disregarding this outlier, the R^2 value increases to 0.963. Calculated shifts were rescaled by a factor of 0.886 and shifted 265.08 ppm to align with experimental results.

The scaling factors and reference shifts found using the PBE functional (see Supplementary Information) are reasonable when compared to previously reported ^{31}P GIPAW results for a set of aluminophosphates.[26] However, as the scaling factor and reference shift seems to be partially dependent upon the GGA functional used, values obtained using the PBEsol functional differ from these previously reported results.

Significant improvement was observed when chemical shift tensors were computed for relaxed structures with rigid unit cell parameters taken from experiment, with an R^2 value of 0.984, as shown in Figure 3. This improved marginally to 0.987 when the lattice parameters were allowed to relax. It is obvious that although geometric relaxations alter the crystallographic structure

Table 1 Unit cell parameters for $Ca(H_2PO_4)_2$ and α–$CaZn_2(PO_4)_2$ as reported in ICSD and fully relaxed structures in italics

Compound	a/Å	b/Å	c/Å	α/°	β/°	γ/°
$Ca(H_2PO_4)_2$	5.550	7.558	8.223	68.154	70.522	86.320
	5.488	*8.037*	*8.410*	*70.882*	*66.212*	*78.39*
α–$CaZn_2(PO_4)_2$	4.960	8.418	8.940	113.75	102.45	94.20
	4.967	*8.412*	*8.937*	*113.688*	*102.340*	*94.254*

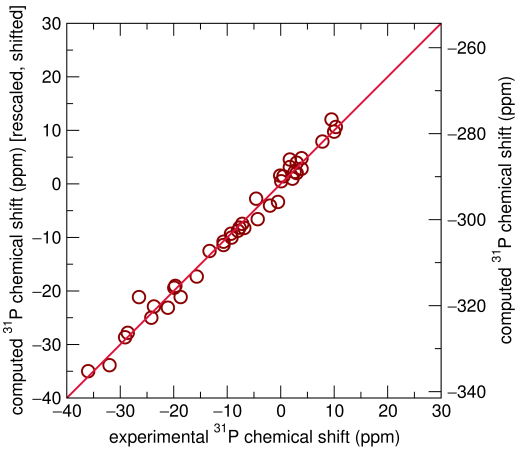

Fig. 3 Calculated isotropic chemical shifts compared with experimental values ($R^2 = 0.984$). The calculations employed X-ray determined lattice parameters but allowed the internal coordinates to be relaxed. Here, the left axis is scaled by a factor of 0.802 and shifted by 234.24 ppm from the VASP calculated shifts.

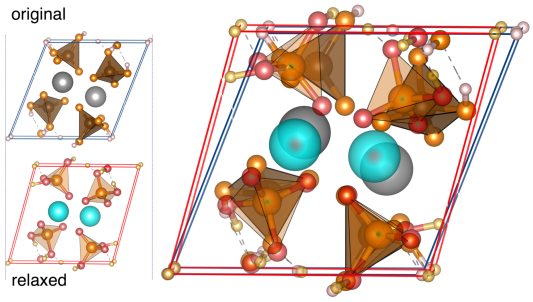

Fig. 4 The crystal structure of $Ca(H_2PO_4)_2$ as reported in ICSD[32] and fully relaxed.

of each compound only minimally, the computation of isotropic chemical shifts is highly sensitive to local environments surrounding the ^{31}P sites, demonstrated most clearly by Li_3PO_4. By extension, this also demonstrates the sensitive nature of NMR to local environments, usually to a greater extent than X-ray diffraction experiments. This is likely to be particularly important in the case of hydrogen and lithium-containing systems, where the X-ray determinations of the light atoms will tend to be poor compared with the computed values. This is supported by previous literature which describes the importance of geometry optimization prior to chemical shift calculations.[53–56]

For complete relaxations, where unit cell parameters were free to optimize, most systems displayed parameters closely matching literature values.† However, $Ca(H_2PO_4)_2$ saw significant lattice parameter distortions upon relaxation. Table 1 includes lattice parameters from ICSD and fully relaxed structures for this compound, along with α–$CaZn_2(PO_4)_2$ for reference. Figure 4 shows the crystal structure of $Ca(H_2PO_4)_2$ as reported by Dickens *et al.* and completely relaxed.[32]

To further support our results, we carried out powder XRD measurements on $Ca(H_2PO_4)_2$, which was obtained by heating $Ca(H_2PO_4)_2 \bullet H_2O$ (99% Strem Chemicals) in a vacuum oven at 200 °C for 3 days. Subsequent Rietveld refinements further confirmed the previously published lattice parameters. Based upon these results, we have given priority to the XRD determined lattice parameters and focus our attention on DFT relaxations with non-variant lattice parameters. We relaxed the $Ca(H_2PO_4)_2$ structure again while taking into account dispersion interactions, however significant lattice parameter deviations were still observed. Previous work on aluminophosphates found that the inclusion of dispersion effects did not necessarily lead to a significantly stronger correlation between experimental and computed ^{31}P chemical shifts, although in some cases it led to optimized geometries which more closely alligned with diffraction determined structures,[26] which is not the case here.

Interestingly GIPAW chemical shift calculations on fully relaxed structures, including $Ca(H_2PO_4)_2$, where the agreement between experiment and calculated lattice parameters is poor (Table 1), nevertheless exhibit strong correlations with experimentally determined NMR chemical shifts, more so than the originally reported structures.† This implies that computed nearest-neighbor ordering information can still be reliable even if the fit to the cell parameters is relatively poor, and it is these interactions which most strongly determine chemical shifts.

NMR line-widths of solids tend to be rather broad due to a combination of interactions, including dipole–dipole, chemical shift anisotropy (CSA), and quadrupolar interactions. However, these interactions, being orientationally dependent, can be at least partially averaged out through magic angle spinning (MAS), which narrows observed line-widths and enhances resolution, while also creating spinning sidebands in the observed spectrum. In solid-state NMR experiments, higher resolution spectra require fast MAS speeds which can eliminate visible spinning sidebands and isolate the NMR peak located at the isotropic chemical shift for a particular crystallographic site. This however leads to an inherent loss of information as the spinning sidebands contain valuable information on the CSA. It should be noted that high resolution solid-state NMR spectra can only be achieved with spin $I = \frac{1}{2}$ nuclei, such as ^{31}P, or if C_q is small.

The experimentally determined CSA tensors for four of the 22 phosphate compounds, $Mg_3(PO_4)_2$, α–$CaZn_2(PO_4)_2$, α–$Zn_3(PO_4)_2$, and β–$Zn_3(PO_4)_2$, containing a total of six distinct phosphorous sites, have been previously reported through the analysis of sideband patterns.[57] We compare these to the GIPAW

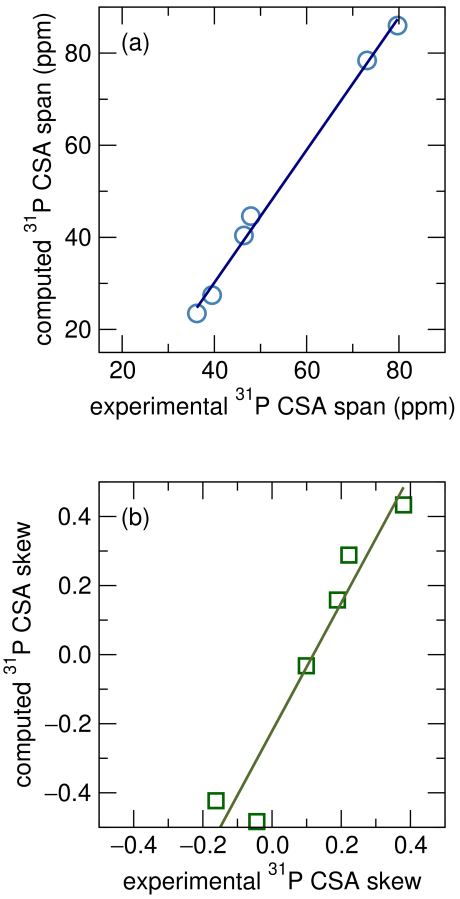

Fig. 5 GIPAW calculated CSA span (a) and skew(b) using relaxed structures with rigid cell parameters compared to experimentally reported values. $R^2 = 0.995$, $R^2 = 0.922$ for span and skew linear regressions, respectively.

computed CSA parameters of the relaxed structures with rigid cell parameters. Computations for the span and skew, shown in Figures 5(a) and (b) show good agreement with experimentally determined values. This has the potential to be useful for spectral assignment for compounds which contain multiple crystallographic ^{31}P sites with similar isotropic shifts when computed isotropic shifts for the sites fall within the bounds of uncertainty, as has previously been done for some aluminophosphate framework materials.[58]

4 Conclusions

As NMR has become widely used in the study of inorganic solids, the challenge of making spectral assignments becomes a non-trivial task. The GIPAW method allows for the calculation of the full second-rank chemical shift tensor for periodic systems. In all comparisons of GIPAW chemical shifts with experimental data (Figures 2, 3, and 5), it can be seen that computed and experimentally derived CSA parameters, while displaying a linear relationship, require rescaling and shifting. This in keeping with prior reports for isotropic chemical shifts;[59–61] and it is clear that this phenomena extends to the CSA span and skew parameters as well. Importantly, this does not detract from the utility of the GIPAW method for NMR spectral assignment. The complete CSA tensor contains valuable and often underutilized information which can be used in NMR spectral analysis and in the developing field of NMR crystallography.

While DFT structure optimizations can lead to errors in lattice parameter predictions, highly localized environments are well predicted via structural relaxation, as demonstrated by the improvement of the isotropic chemical shift predictions in the relaxed structures. This is especially surprising as DFT relaxations are done while neglecting thermal effects, effectively at 0 K. We have shown that GIPAW computations show clear improvement in the ^{31}P isotropic chemical shifts calculated from relaxed structures rather than from XRD-determined structures, establishing that the calculated fractional coordinates of these older structures containing oxygen and other light atoms are more reliable than those reported experimentally. This effect could stem from the short nature of the P–O bond lengths inherent in phosphate systems, making the ^{31}P chemical shifts less sensitive to thermal effects. On the other hand, the relaxation of the unit cell parameters, which are less accurate in DFT calculations, has only a minor effect on the calculated NMR shifts, at least for the phosphate systems studied here.

Conflicts of interest

There are no conflicts to declare.

Acknowledgements

We acknowledge the Ras al Khaimah Centre for Advanced Materials and the National Science Foundation [(MRSEC, NSF DMR 172025 (IRG-1)] for partial support, and computing infrastructure supported through NSF DMR 1720256 and NSF CNS 1725797.

Notes and references

1 A. K. Cheetham, N. J. Clayden, C. M. Dobson and R. J. B. Jakeman, *Chem. Commun.*, 1986, 195.
2 K. A. Smith, R. J. Kirkpatrick, E. Oldfield and D. M. Henderson, *Am. Mineral.*, 1983, **68**, 1206–1215.
3 A. R. Ferreira, E. Küçükbenli, A. A. Leitão and S. de Gironcoli, *Phys. Rev. B*, 2011, **84**, 235119.
4 A. Knappschneider, C. Litterscheid, N. C. George, J. Brgoch, N. Wagner, J. Beck, J. A. Kurzman, R. Seshadri and B. Albert, *Angew. Chem. Int. Ed.*, 2014, **53**, 1684–1688.
5 G. Henkelman, A. Arnaldsson and H. Jónsson, *Comp. Mater. Sci.*, 2006, **36**, 354–360.
6 S. T. Holmes, R. J. Iuliucci, K. T. Mueller and C. Dybowski, *J. Chem. Phys.*, 2014, **141**, 164121.
7 S. T. Holmes, R. J. Iuliucci, K. T. Mueller and C. Dybowski, *J. Chem. Theory Comp.*, 2015, **11**, 5229–5241.
8 J. Weber and J. Schmedt auf der Günne, *Phys. Chem. Chem. Phys.*, 2010, **12**, 583–603.
9 C. J. Pickard and F. Mauri, *Phys. Rev. B*, 2001, **63**, 245101.
10 J. R. Yates, C. J. Pickard and F. Mauri, *Phys. Rev. B*, 2007, **76**, 1–11.
11 T. Gregor, F. Mauri and R. Car, *J. Chem. Phys.*, 1999, **111**, 1815–1822.

12 T. Charpentier, *Solid State Nuc. Magn. Res.*, 2011, **40**, 1–20.

13 M. Profeta, F. Mauri and C. J. Pickard, *J. Am. Chem. Soc.*, 2003, **125**, 541–548.

14 S. E. Ashbrook, L. Le Pollès, R. Gautier, C. J. Pickard and R. I. Walton, *Phys. Chem. Chem. Phys.*, 2006, **8**, 3423–3431.

15 J. R. Yates, C. J. Pickard, M. C. Payne, R. Dupree, M. Profeta and F. Mauri, *J. Phys. Chem. A*, 2004, **108**, 6032–6037.

16 L. Shao, J. R. Yates and J. J. Titman, *J. Phys. Chem. A*, 2007, **111**, 13126–13132.

17 M. Choi, K. Matsunaga, F. Oba and I. Tanaka, *J. Phys. Chem. C*, 2009, **113**, 3869–3873.

18 F. Vasconcelos, S. Cristol, J. F. Paul, L. Montagne, F. Mauri and L. Delevoye, *Magnetic Resonance in Chemistry*, 2010, **48**, S142–S150.

19 F. Pourpoint, C. Gervais, L. Bonhomme-Coury, T. Azaïs, C. Coelho, F. Mauri, B. Alonso, F. Babonneau and C. Bonhomme, *Appl. Magn. Res.*, 2007, **32**, 435–457.

20 F. Pourpoint, C. Gervais, L. Bonhomme-Coury, F. Mauri, B. Alonso and C. Bonhomme, *Comptes Rendus Chimie*, 2008, **11**, 398–406.

21 G. Girard, F. Vasconcelos, L. Montagne and L. Delevoye, *Solid State Nucl. Magn. Res.*, 2017, **84**, 210–215.

22 C. Bonhomme, C. Gervais, C. Coelho, F. Pourpoint, T. Azaïs, L. Bonhomme-Coury, F. Babonneau, G. Jacob, M. Ferrari, D. Canet, J. R. Yates, C. J. Pickard, S. A. Joyce, F. Mauri and D. Massiot, *Magnetic Resonance in Chemistry*, 2010, **48**, S86–S102.

23 D. M. Dawson and S. E. Ashbrook, *Journal of Physical Chemistry C*, 2014, **118**, 23285–23296.

24 H. Chappell, M. Duer, N. Groom, C. Pickard and P. Bristowe, *Physical Chemistry Chemical Physics*, 2008, **10**, 600–606.

25 C. Gervais, C. Coelho, T. Azaïs, J. Maquet, G. Laurent, F. Pourpoint, C. Bonhomme, P. Florian, B. Alonso, G. Guerrero, P. H. Mutin and F. Mauri, *Journal of Magnetic Resonance*, 2007, **187**, 131–140.

26 S. Sneddon, D. M. Dawson, C. J. Pickard and S. E. Ashbrook, *Physical Chemistry Chemical Physics*, 2014, **16**, 2660–2673.

27 G. Kresse and J. Hafner, *Phys Rev. B*, 1993, **48**, 13115–13118.

28 G. Kresse and J. Furthmüller, *Phys Rev. B*, 1996, **54**, 11169–11186.

29 J. P. Perdew, A. Ruzsinszky, G. I. Csonka, O. a. Vydrov, G. E. Scuseria, L. a. Constantin, X. Zhou and K. Burke, *Phys. Rev. Lett.*, 2008, **100**, 136406.

30 N. I. P. Ayu, E. Kartini, L. D. Prayogi, M. Faisal and Supardi, *Ionics*, 2016, **22**, 1051–1057.

31 C. Calvo and P. K. L. Au, *Canadian J. Chem.*, 1969, **47**, 3409–3416.

32 B. Dickens, E. Prince, L. W. Schroeder and W. E. Brown, *Acta Crystallogr. B*, 1973, **29**, 2057–2070.

33 C. Calvo, *Canadian J. Chem.*, 1965, **43**, 436–445.

34 K. Y. Leung and C. Calvo, *Canadian J. Chem.*, 1972, **50**, 2519–2526.

35 R. J. B. Jakeman and A. K. Cheetham, *J. Am. Chem. Soc.*, 1988, **110**, 1140–1143.

36 M. T. Averbuch-Pouchot and A. Durif, *Acta Crystallogr. B*, 1979, **35**, 151–152.

37 J. S. Stephens and C. Calvo, *Canadian J. Chem.*, 1967, **45**, 2303–2316.

38 L. W. Schroeder, E. Prince and B. Dickens, *Acta Crystallogr. B*, 1975, **31**, 9–12.

39 N. A. Curry and D. W. Jones, *J. Chem. Soc. A*, 1971, 3725–3729.

40 A. G. Nord, *Mater. Res. Bull.*, 1977, **12**, 563–568.

41 S. Boudin, A. Grandin, M. M. Borel, A. Leclaire and B. Raveau, *Acta Crystallogr.*, 1993, **49**, 2062–2064.

42 C. Calvo, *Inorg. Chem.*, 1968, **7**, 1345–1351.

43 A. G. Nord and P. Kierkegaard, *Acta Chem. Scand. A*, 1968, **22**, 1466–1474.

44 B. E. Robertson and C. Calvo, *J. Solid State Chem.*, 1970, **1**, 120–133.

45 C. Calvo, *Acta Crystallogr.*, 1967, **23**, 289–295.

46 J. Alkemper, H. Paulus and H. Fueß, *Z. Kristallogr.*, 1994, **209**, 616.

47 K. N. Ng and C. Calvo, *Canadian J. Chem.*, 1973, **51**, 2613–2620.

48 L. O. Hagman, I. Jansson and C. Magnéli, *Acta Chem. Scand.*, 1968, **22**, 1419–1429.

49 L.-O. Hagman and P. Kierkegaard, *Acta Chem. Scand.*, 1968, **22**, 1822–1832.

50 A. G. Nord and K. B. Lindberg, *Acta Chem. Scand. A*, 1975, **29**, 1–6.

51 B. P. Onac and H. S. Effenberger, *Am. Mineral.*, 2007, **92**, 1998–2001.

52 R. K. Harris, P. Hodgkinson, C. J. Pickard, J. R. Yates and V. Zorin, *Encyclopedia of Magnetic Resonance*, 2009.

53 C. Bonhomme, C. Gervais, F. Babonneau, C. Coelho, F. Pourpoint, T. Azaïs, S. E. Ashbrook, J. M. Griffin, J. R. Yates, F. Mauri and C. J. Pickard, *Chemical Reviews*, 2012, **112**, 5733–5779.

54 F. Vasconcelos, S. Cristol, J.-f. Paul, G. Tricot, J.-p. Amoureux, L. Montagne, F. Mauri and L. Delevoye, *Inorganic Chemistry*, 2008, **47**, 7327–7337.

55 S. E. Ashbrook and D. McKay, *Chemical Communications*, 2016, **52**, 7186–7204.

56 G. Kieslich, A. C. Forse, S. Sun, K. T. Butler, S. Kumagai, Y. Wu, M. R. Warren, A. Walsh, C. P. Grey and A. K. Cheetham, *Chem. Mater.*, 2016, **28**, 312–317.

57 R. J. B. Jakeman, *PhD thesis*, University of Oxford, 1986.

58 D. M. Dawson, R. F. Moran, S. Sneddon and S. E. Ashbrook, *Magn. Res. Chem.*, 2018, 1–15.

59 J. M. Griffin, J. R. Yates, A. J. Berry, S. Wimperis and S. E. Ashbrook, *J. Am. Chem. Soc.*, 2010, **132**, 15651–15660.

60 S. E. Ashbrook, D. M. Dawson and J. M. Griffin, *Local Structural Characterisation*, John Wiley & Sons, Ltd, Chichester, UK, 2013, pp. 1–88.

61 A. Zheng, S. B. Liu and F. Deng, *J. Phys. Chem. C*, 2009, **113**, 15018–15023.

Supporting information for:

Ab initio computation for solid-state ^{31}P NMR of inorganic phosphates: Revisiting X-ray structures†

E-mail:

Kartik Pilar,[a] Zeyu Deng,[b] Molleigh B. Preefer,[a,c] Joya A. Cooley,[a] Raphaële Clément,[a,d] Ram Seshadri,[a,c,d] and Anthony K. Cheetham[a,e*]

[a]*Materials Research Laboratory*

University of California, Santa Barbara, California 93106 United States.

[b]*Department of Materials Science and Metallurgy, University of Cambridge*

27 Charles Babbage Rd, CB3 0FS Cambridge, UK.

[c]*Department of Chemistry and Biochemistry*

University of California, Santa Barbara, California 93106 United States.

[d]*Materials Department*

University of California, Santa Barbara, California 93106 United States.

[e]*Department of Materials Science and Engineering*

National University of Singapore, 117575 Singapore.

*E-mail: akc30@cam.ac.uk

Gamma centered k-point grids were created using automated k-mesh generation, built into the VASP code. The density of k-points was determined by the formula:

$$N_x = max(1, l \times |\vec{b_x}| + 0.5) \tag{1}$$

where N_x is the number of k-points along the reciprocal lattice vector, $\vec{b_x}$, corresponding to lattice vector $\vec{x}$. l is the input length parameter which dictates k-spacing, which was found to converge at 15. Larger values for l correspond to greater k-point densities.

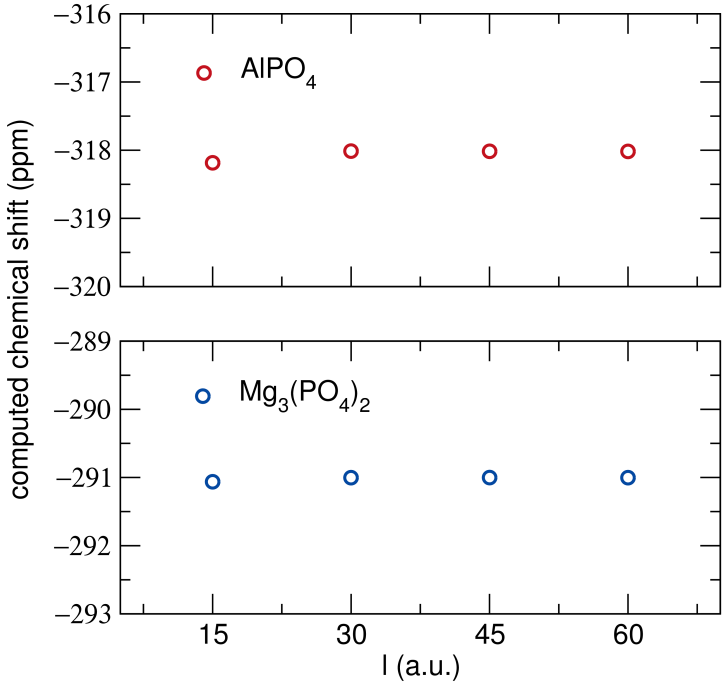

Figure S1: k-spacing was tested for convergence with $AlPO_4$ and $Mg_3(PO_4)_2$.

Table S1: Unit cell parameters for 22 inorganic phosphate compounds studied in this work as reported in ICSD and fully relaxed structures below in italics

Compound	a/Å	b/Å	c/Å	α/°	β/°	γ/°
Li_3PO_4	4.924	6.115	10.473	90	90	90
	4.974	*6.141*	*10.538*	*90*	*90*	*90*
$Cd_2P_2O_7$	6.623	6.672	6.858	64.62	84.20	82.38
	6.659	*6.619*	*6.807*	*64.950*	*84.087*	*82.011*
$Ca(H_2PO_4)_2$	5.550	7.558	8.223	68.154	70.522	86.320
	5.488	*8.037*	*8.410*	*70.882*	*66.212*	*78.39*
α–$Zn_3(PO_4)_2$	8.14	5.63	15.04	90	105.13	90
	8.215	*5.618*	*15.120*	*90*	*105.046*	*90*
$Na_4P_2O_7$	9.367	5.390	13.480	90	90	90
	9.324	*5.393*	*13.499*	*90*	*90*	*90*
α–$CaZn_2(PO_4)_2$	4.96	8.42	8.94	113.75	102.45	94.20
	4.967	*8.412*	*8.937*	*113.688*	*102.340*	*94.254*
$KZn_4(PO_4)_3$	8.166	9.675	13.810	90	90	90
	8.168	*9.627*	*13.854*	*90*	*90*	*90*
β–$Zn_3(PO_4)_2$	8.270	8.686	9.170	90	90	12.771
	8.270	*8.716*	*9.152*	*90*	*90*	*113.132*
$Ca(H_2PO_4)_2 \bullet (H_2O)$	5.626	6.256	11.889	92.928	96.656	114.229
	5.585	*6.208*	*11.785*	*92.942*	*95.760*	*114.357*
$CaHPO_4 \bullet 2(H_2O)$	5.812	15.180	6.239	90	116.430	90
	5.796	*14.861*	*6.084*	*90*	*115.780*	*90*
$MgZn_2(PO_4)_2$	7.569	8.355	5.059	90	94.95	90
	7.585	*8.314*	*5.061*	*90*	*95.142*	*90*
β–$Ca_2P_2O_7$	6.686	6.686	24.147	90	90	90
	6.664	*6.664*	*24.104*	*90*	*90*	*90*
α–$Ca_2P_2O_7$	5.315	8.542	12.660	90	90.3	90
	5.323	*8.483*	*12.641*	*90*	*89.845*	*90*
$Mg_3(PO_4)_2$	8.512	8.982	9.320	116.34	91.50	114.49
	8.504	*8.982*	*9.325*	*115.944*	*91.356*	*114.378*
α–$Zn_2P_2O_7$	8.259	9.099	10.618	99.350	112.888	90
	8.272	*9.129*	*10.663*	*99.027*	*112.822*	*112.822*
α–$Mg_2P_2O_7$	6.981	8.295	9.072	90	113.999	90
	6.954	*8.300*	*9.067*	*90*	*113.856*	*90*
$NaAlP_2O_7$	7.203	7.710	9.326	90	111.743	90
	7.227	*7.694*	*9.335*	*90*	*111.761*	*90*
$KAlP_2O_7$	7.308	8.025	9.662	90	90	106.69
	7.339	*8.081*	*9.684*	*90*	*90*	*107.096*
α–$Sr_2P_2O_7$	5.404	8.910	13.105	90	90	90
	5.372	*8.899*	*13.151*	*90*	*90*	*90*
$NaZr_2(PO_4)_2$	8.804	8.804	9.132	61.179	61.179	60
	8.855	*8.855*	*9.132*	*60.997*	*60.998*	*60.000*
$Mg_2P_4O_{12}$	7.191	7.191	9.675	98.959	109.792	109.652
	7.195	*7.195*	*9.722*	*99.062*	*109.355*	*109.843*
$AlPO_4$	4.946	4.946	10.953	90	90	120
	4.974	*4.974*	*11.016*	*90*	*90*	*120*

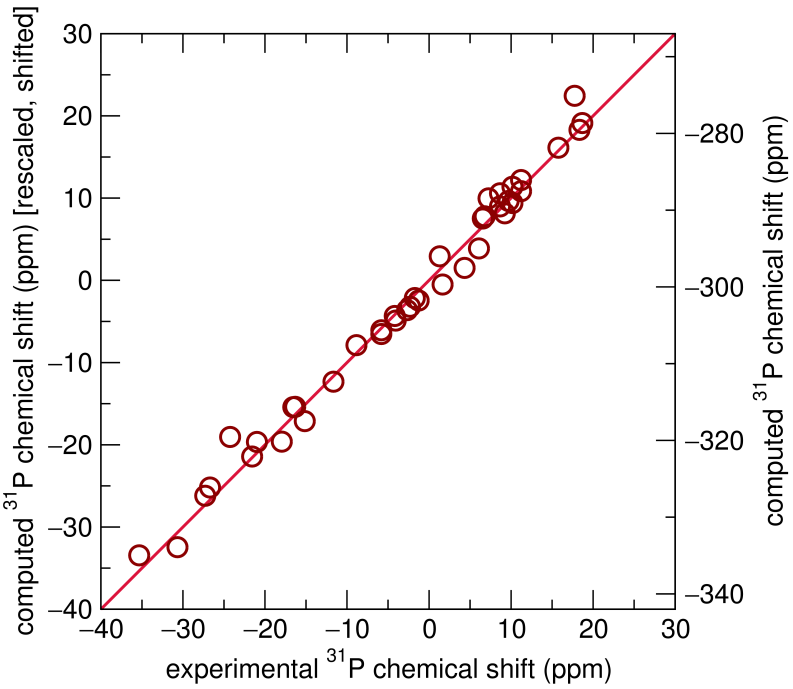

Figure S2: GIPAW calculated isotropic chemical shifts using fully relaxed structures and the PBEsol functional compared to experimentally reported values. $R^2 = 0.987$. Here, the left vertical axis is scaled by a factor of 0.933 and shifted by 299.15 ppm from the VASP calculated shifts.

Due to the large deviations of lattice parameters during the full relaxation of $Ca(H_2PO_4)_2$, another DFT relaxation was done for this structure including dispersion interactions using the DFT-D2 method.[1] The PBE functional[2] was used as the PBEsol functional is incompatible with the DFT-D2 method within the VASP code. Even with dispersion forces accounted for, lattice cell parameters still largely deviated from the previously reported structure, as shown in Table S2.

Table S2: Unit cell parameters for $Ca(H_2PO_4)_2$ as reported in ICSD and fully relaxed while accounting for dispersion interactions below in italics

Compound	a/Å	b/Å	c/Å	α/°	β/°	γ/°
$Ca(H_2PO_4)_2$	5.550	7.558	8.223	68.154	70.522	86.320
	5.490	*7.918*	*8.312*	*70.613*	*67.926*	*79.041*

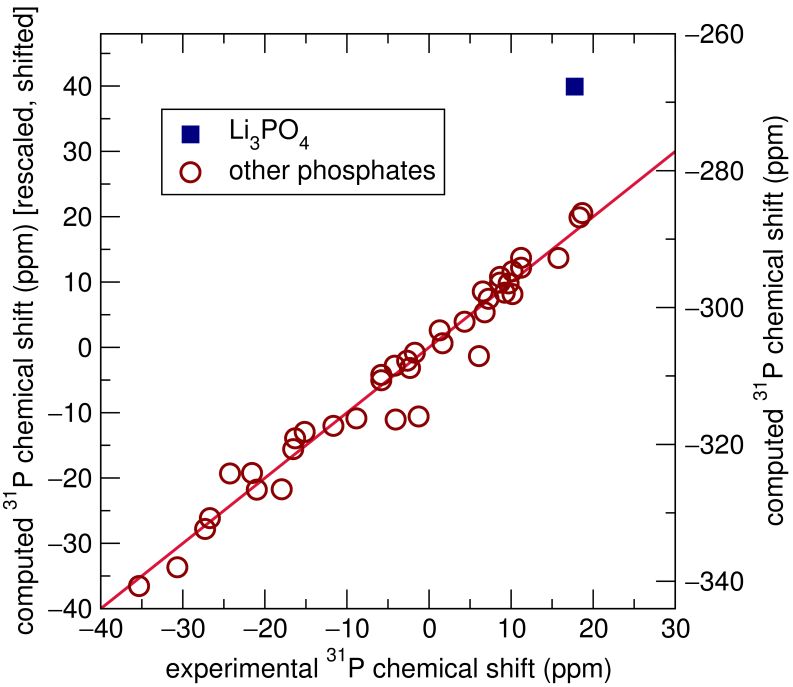

Figure S3: GIPAW calculated isotropic chemical shifts using reported structures from ICSD and the PBE functional compared to experimentally reported values. $R^2 = 0.924$, or $R^2 = 0.963$ if Li_3PO_4 is disregarded. Here, the left vertical axis is scaled by a factor of 1.048 and shifted by 305.80 ppm from the VASP calculated shifts.

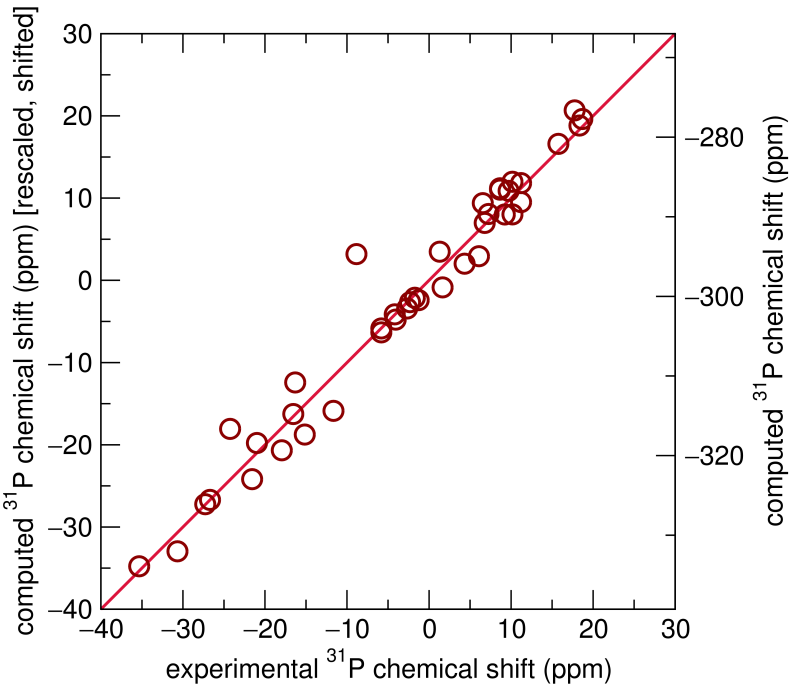

Figure S4: GIPAW calculated isotropic chemical shifts using structures relaxed with rigid cell parameters and the PBE functional compared to experimentally reported values. $R^2 = 0.964$. Here, the left vertical axis is scaled by a factor of 0.968 and shifted by 297.99 ppm from the VASP calculated shifts.

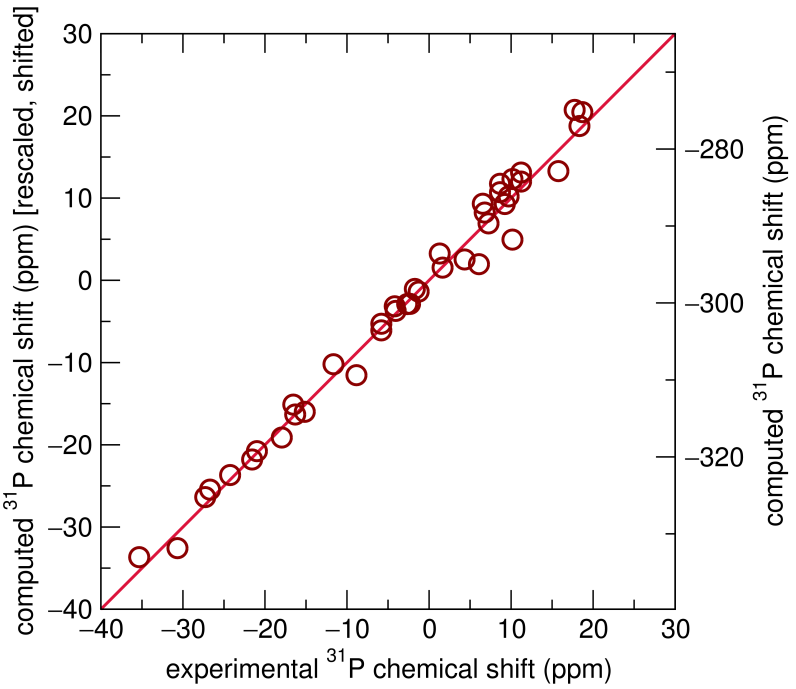

Figure S5: GIPAW calculated isotropic chemical shifts using fully relaxed structures and the PBE functional compared to experimentally reported values. $R^2 = 0.986$. Here, the left vertical axis is scaled by a factor of 0.936 and shifted by 297.05 ppm from the VASP calculated shifts.

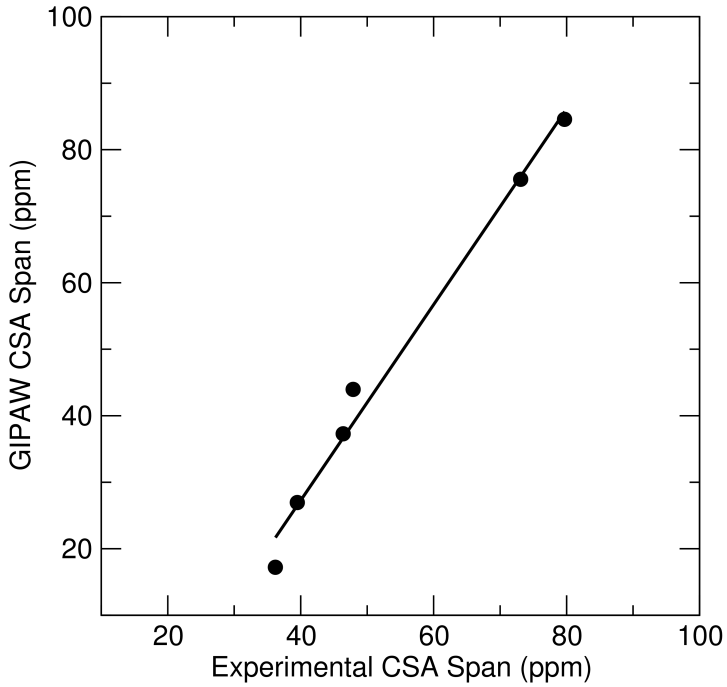

Figure S6: GIPAW calculated CSA span using structures relaxed with rigid lattice parameters and the PBE functional compared to experimentally reported values. $R^2 = 0.987$.

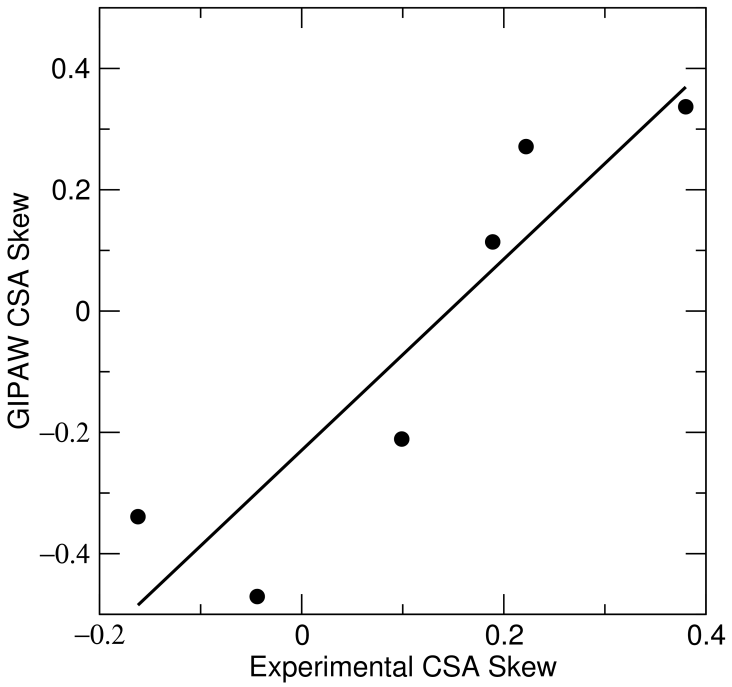

Figure S7: GIPAW calculated CSA skew using structures relaxed with rigid lattice parameters and the PBE functional compared to experimentally reported values. $R^2 = 0.831$.

Table S3: Computed ^{31}P CSA tensor parameters for all 22 compounds computed for structures relaxed with rigid cell parameters using PBEsol and PBE written below in italics.

Compound	δ_{iso}/ppm	Ω/ppm	κ
Li_3PO_4	–276.6878	6.3630	–0.1396
	–276.6414	*6.2621*	*–0.1392*
$Cd_2P_2O_7$	–296.7197	161.3842	–0.5365
	–295.8874	*161.3797*	*–0.5531*
	–299.8709	117.1326	–0.6952
	–298.8751	*116.1794*	*–0.6860*
$Ca(H_2PO_4)_2$	–289.9187	167.5137	0.3432
	–289.6518	*177.1814*	*0.4328*
	–295.8704	140.7196	0.1813
	–294.9645	*143.7031*	*0.1395*
α–$Zn_3(PO_4)_2$	–288.1672	78.4081	0.1582
	–286.7135	*75.5592*	*0.1139*
$Na_4P_2O_7$	–287.7554	143.1338	–0.8727
	–286.5922	*142.5992*	*–0.8725*
	–286.7524	153.2788	–0.8780
	–285.6128	*152.2954*	*–0.8757*
α–$CaZn_2(PO_4)_2$	–290.4665	85.9927	0.2883
	–289.7158	*84.5761*	*0.2712*
	–279.5392	44.6057	–0.4834
	–278.5499	*43.9620*	*–0.4707*
$KZn_4(PO_4)_3$	–288.8791	66.8469	–0.6744
	–286.7518	*64.8321*	*–0.6802*
	–278.4310	73.0178	0.3885
	–277.7230	*74.5302*	*0.3547*
β–$Zn_3(PO_4)_2$	–289.1686	23.4822	–0.0323
	–289.7030	*17.2178*	*–0.2111*
	–281.8146	40.4123	–0.4229
	–280.8441	*37.2953*	*–0.3990*
$Ca(H_2PO_4)_2 \bullet (H_2O)$	–295.1250	124.8185	–0.1526
	–294.3918	*131.1878*	*–0.1121*
	–289.7484	103.1896	0.2026
	–288.2935	*103.1762*	*0.0475*
$CaHPO_4 \bullet 2(H_2O)$	–285.9999	116.8827	0.0249
	–286.4263	*123.1148*	*–0.0670*
$MgZn_2(PO_4)_2$	–285.7051	47.6715	–0.2044
	–285.7744	*47.6568*	*–0.1395*
β–$Ca_2P_2O_7$	–305.8869	174.8703	–0.1685
	–304.5263	*172.4847*	*–0.1742*
	–300.9802	141.3152	–0.5608
	–300.1662	*140.7336*	*–0.5560*
	–302.5808	149.4955	–0.6724
	–301.5242	*148.3881*	*–0.6700*
	–303.2678	145.1390	–0.4339
	–302.2609	*144.7101*	*–0.4379*

Table S4: Computed ^{31}P CSA tensor parameters for all 22 compounds computed for structures relaxed with rigid cell parameters using PBEsol and PBE written below in italics (continuted)

Compound	δ_{iso}/ppm	Ω/ppm	κ
α–$Ca_2P_2O_7$	–301.8591	125.2659	–0.3203
	–300.7201	*123.1066*	*–0.3024*
	–305.1167	123.8306	–0.5170
	–304.0286	*123.9809*	*–0.5428*
$Mg_3(PO_4)_2$	–291.0622	27.4465	0.4335
	–290.7743	*26.9534*	*0.3368*
α–$Zn_2P_2O_7$	–317.9956	135.5742	–0.3852
	–317.3484	*135.0370*	*–0.4140*
	–320.4896	144.9354	–0.3686
	–319.3358	*144.2677*	*–0.3910*
	–313.2307	113.1426	–0.7932
	–314.3873	*115.2942*	*–0.7677*
α–$Mg_2P_2O_7$	–315.3940	146.4777	–0.6315
	–294.6839	*218.8990*	*–0.2985*
	–307.2805	110.9000	–0.9052
	–310.8127	*160.9620*	*–0.2276*
$NaAlP_2O_7$	–315.8403	150.6109	–0.3564
	–314.7761	*149.1990*	*–0.3615*
	–326.3221	130.6143	–0.5731
	–325.5653	*130.1871*	*–0.5751*
$KAlP_2O_7$	–320.1908	112.9544	–0.9751
	–318.4101	*112.4001*	*–0.9479*
	–327.3605	133.2534	–0.2466
	–326.1127	*132.3035*	*–0.2410*
α–$Sr_2P_2O_7$	–304.1691	121.4014	–0.8373
	–302.9232	*119.5529*	*–0.8764*
	–301.9383	109.7637	–0.5855
	–300.4661	*106.8719*	*–0.5980*
$NaZr_2(PO_4)_2$	–322.8137	13.9623	–0.9348
	–322.9771	*16.2592*	*–0.7897*
$Mg_2P_4O_{12}$	–333.8429	230.9511	0.4928
	–332.0204	*230.4921*	*0.4886*
	-335.3001	241.2628	0.5337
	–333.9006	*240.7955*	*0.5354*
$AlPO_4$	–318.0154	8.5019	0.0751
	–316.6491	*9.0072*	*0.0174*

References

(1) S. Grimme, *J. Comput. Chem.*, 2006, **27**, 1787.

(2) J. Perdew, K. Burke, M. Ernzerhof, *Phys. Rev. Lett.*, 1996, **77**, 3865-3868.